Molecular Crystals
Publication details, including instructions for authors and subscription information:
http://www.tandfonline.com/loi/gmcl15

Some Electronic and Chemical Consequences of Non-basal Dislocations in Crystalline Anthracene

J. M. Thomas [a] & J. O. Williams [a]
[a] Department of Chemistry, University College of North Wales, Bangor, Wales, U.K.
Version of record first published: 21 Mar 2007.

To cite this article: J. M. Thomas & J. O. Williams (1969): Some Electronic and Chemical Consequences of Non-basal Dislocations in Crystalline Anthracene, Molecular Crystals, 9:1, 59-79

To link to this article: http://dx.doi.org/10.1080/15421406908082733

5

Some Electronic and Chemical Consequences of Non-basal Dislocations in Crystalline Anthracene

J. M. THOMAS and J. O. WILLIAMS

Department of Chemistry,
University College of North Wales,
Bangor, Wales, U.K.

Abstract—Efforts have been made to detect and characterize individual dislocations, small-angle boundaries and extended (nonequilibrium) lattice vacancies, formed by the annihilation of dislocations, in single crystals of anthracene. Only those dislocations emergent at the basal (00*l*) faces may be identified using the dislocation-etch-pit technique; but some information regarding dislocations which glide in the basal plane may be deduced from deformation and cleavage studies. Three distinct kinds of experiments have been carried out on a variety of crystals, the dislocation content of which ranges from 10^2 cm^{-2} (for vapor-grown) to 10^8 cm^{-2} (for deformed melt-grown crystals).

From studies of thermally stimulated currents, it is confirmed that the peak in the " glow " curve centered at around 273 °K, corresponding to a positive hole trap of depth 0.7 eV, is an indigenous feature of highly purified crystalline anthracene. It is established that, somewhat surprisingly, the magnitude of this " glow " peak decreases with increasing density of non-basal dislocations.

Studies of space-charge-limited-currents, using an injector electrode, yield a more complete picture of the trapping centers; and it is found that the total concentration of traps is directly proportional to the density of non-basal dislocations. By making reasonable estimates of the radius of " distortion " at dislocation cores, and by assuming that all molecules situated within this distorted region may function as trapping centers, it is possible to account for the observed trap densities, which range from 10^{13} to 10^{19} cm^{-3} depending on the origin and pretreatment of the particular crystal.

A direct test of one chemical consequence of the existence of dislocations in anthracene was made by studying, using optical microscopy, the transformation of the solid into dipara-anthracene, by photolysis with UV light. The dimerization is favored at dislocation cores, a fact of some significance for the general study of organic solid-state reactions, particularly in the context of topochemistry.

1. Introduction

The recent spate of papers[1-6] dealing with the deformation, morphology, cleavage and etching characteristics of single crystals of anthracene has at last provided a reasonable crystallographic foundation for describing the nature of the dislocations which have long been postulated to occur in this solid. Although a clear pattern seems to have emerged already, we shall not be absolutely certain of the various glide planes and Burgers vectors of the dislocations until a systematic transmission electron microscopic study is carried out. This technique alone seems to be capable of yielding information concerning basal dislocations. It may, however, as with other materials,[7] turn out to be much less informative about non-basal dislocations, upon which we shall concentrate in this paper.

Section 2 summarizes the evidence, derived chiefly from topographical studies of etched and cleaved surfaces, for the characterization of various kinds of sessile non-basal dislocations in anthracene. It also draws particular attention to two distinct kinds of edge dislocations which may be introduced into the lattice by different methods of deformation. Section 3 summarizes the results of electrical measurements designed to examine the role of dislocations as (electronic) trapping centers. And the last section describes a straightforward chemical consequence of how the reactivity of a solid is affected by the disorder associated with dislocation cores.

2. Detection and Characterization of Dislocations

Using procedures developed by Gilman and others,[8-11] it is possible[12] to identify many of the dislocations, the regions of emergence‡ of which are revealed by dissolution etching (see ref. 12 for experimental details). At first sight, it appears that the only information extractable from the dislocation-etch technique is either (i) that the dislocation responsible for the pit has a component of its Burgers vector perpendicular to the basal (00l) planes, or, (ii), that the vector lies in the basal plane but the dislocation itself is inclined to the plane (as with a non-basal edge dislocation). However, from the observed alignments of dislocation etch pits in deformed samples (compare

‡ We are, throughout, referring to emergence of dislocations at (00l), basal, faces.

ref. 13), the preferred planes in which dislocation loops glide, and the " river-line " patterns on cleavage faces, it is possible to characterize, with reasonable confidence, the nature of the dislocations present. This approach enables both the possible glide plane and the direction (but not the magnitude) of the Burgers vector to be deduced.

From the occurrence of traces of tilt boundaries in the [100] direction on (00l) faces, there is little doubt[4,12] that basal dislocations of the type (001) [010] exist in anthracene. The slip system (010) [001] is also much favoured and gives rise to screw dislocations emergent at basal faces. The (100) [010] slip system, although apparently less feasible from a qualitative analysis of molecular projections on (100) planes, has been shown to be active, and it gives rise to edge dislocations emergent at (00l) faces. To account for asymmetrical tilt boundaries and symmetrical twist boundaries intersecting basal faces, we have to consider dislocations of the type (010) [100] in combination with those designated (100) [010] and (010) [001] respectively. In this Section, we draw particular attention to non-basal edge dislocations. It will transpire that, as well as those arising from (100) [010], there is also evidence for the existence of (20$\bar{1}$) [010] type of dislocation.

2.1. Experimental Details

Cleavage faces of high-purity, melt-grown[12] crystals of anthracene were etched with oleum, as described[12] previously. The etch patterns were examined before and after deformation, which was carried out in three ways: (i) two parallel stainless-steel plates, which could be tightened with a screw, served to compress the crystals on opposite (010) faces. The extent of deformation itself was not recorded, but the increase in the density of dislocations could be evaluated quantitatively from the subsequent etching; (ii) point indentation of (00l) faces was performed using a sharp needle; and, (iii) the crystals could be cut, through the (00l) planes, with a stainless-steel blade.

2.2. The " As-grown " Crystals

Figure 1 is a typical optical micrograph of a cleaved (00l) face of an anthracene crystal etched in oleum. Two important features are

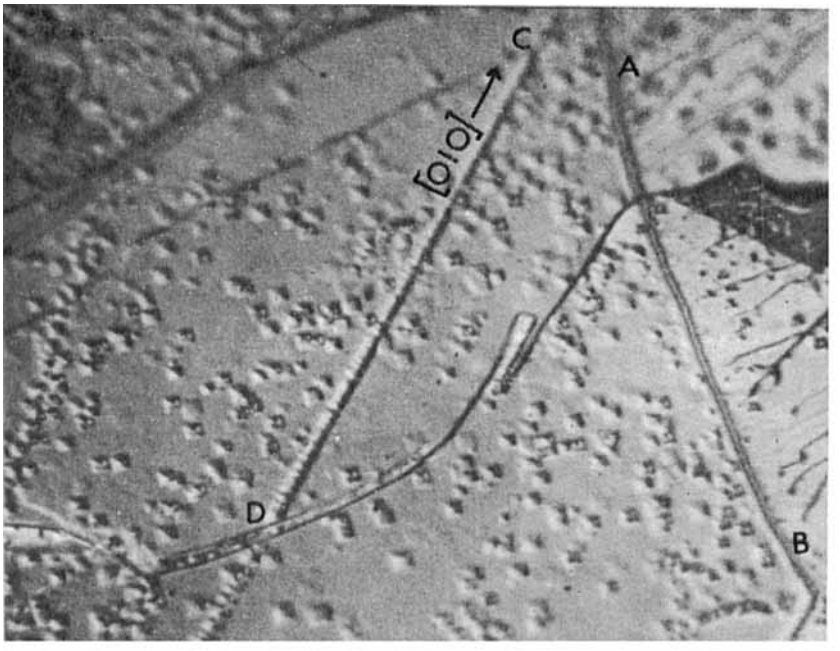

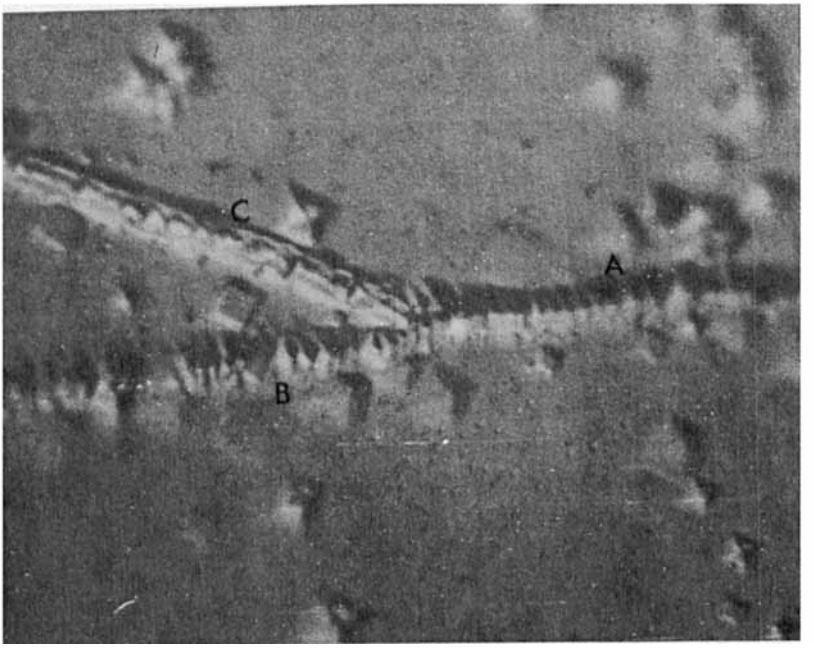

Figure 1. Optical micrograph of a (00*l*) face of a cleaved anthracene crystal etched with oleum. *AB* delineates a twist boundary, whereas *CD* is a row of etch pits at the emergence points of edge dislocations. (× 300)

Figure 2. Intersecting tilt boundaries *A*, *B* and *C* used to test Frank's formula. (× 1000)

apparent. AB is a curvilinear row of closely-spaced etch pits from which emerges a river-line pattern of cleavage steps. The row delineates a twist boundary consisting of screw dislocations emergent at the $(00l)$ face. Since it is curvilinear, a few edge dislocations, also emergent at $(00l)$ faces, must be associated with the boundary. A row of closely-spaced etch pits CD runs along the [010] direction. No cleavage steps emerge from this row of pits. These etch pits demarcate the emergence points of edge dislocations aligned in their slip planes, the Burgers vector being in the [010] direction. Several slip planes are possible, all of which must be of the type $\{h0l\}$. But, from an examination of the crystal structure, two particular types of planes are more favourable than the others (100) and $(20\bar{1})$.

Many intersecting small-angle boundaries, consisting principally of non-basal edge dislocations, are seen (see Fig. 2) in melt-grown crystals which have a well-developed mosaic structure. Although the algebraic sum of the linear densities, n_A, n_B, and n_C, of etch pits in such y-shaped boundaries is often zero, it is not always possible to use Frank's theorem[14] rigorously to establish that such arrays are composed of pure edge dislocations, because the values of the angles ϕ between each array and the nearest slip direction cannot be determined sufficiently well to be used in the equation:

$$\frac{n_A}{\cos\phi_A} = \frac{n_B}{\cos\phi_B} + \frac{n_C}{\cos\phi_C} \tag{1}$$

For melt-grown samples, the dislocation content varies from sample to sample but generally falls in the range of 10^5 to 10^6 cm.$^{-2}$ in contrast to the solution-grown and vapour-grown samples which have contents of 10^3 to 10^4 and 10^2 cm.$^{-2}$ respectively.

2.3. Deliberately Deformed Crystals

It has been consistently noted that, depending on the precise manner of deformation, aligned dislocations of two different kinds may be introduced to the lattice. Figure 3 shows an etched cleavage face of an anthracene crystal deformed by compression perpendicular to opposite (010) faces. The larger pits are nucleated at sessile dislocations randomly distributed throughout the solid; whereas the smaller ones, which have a strong tendency to be aligned in the [010]

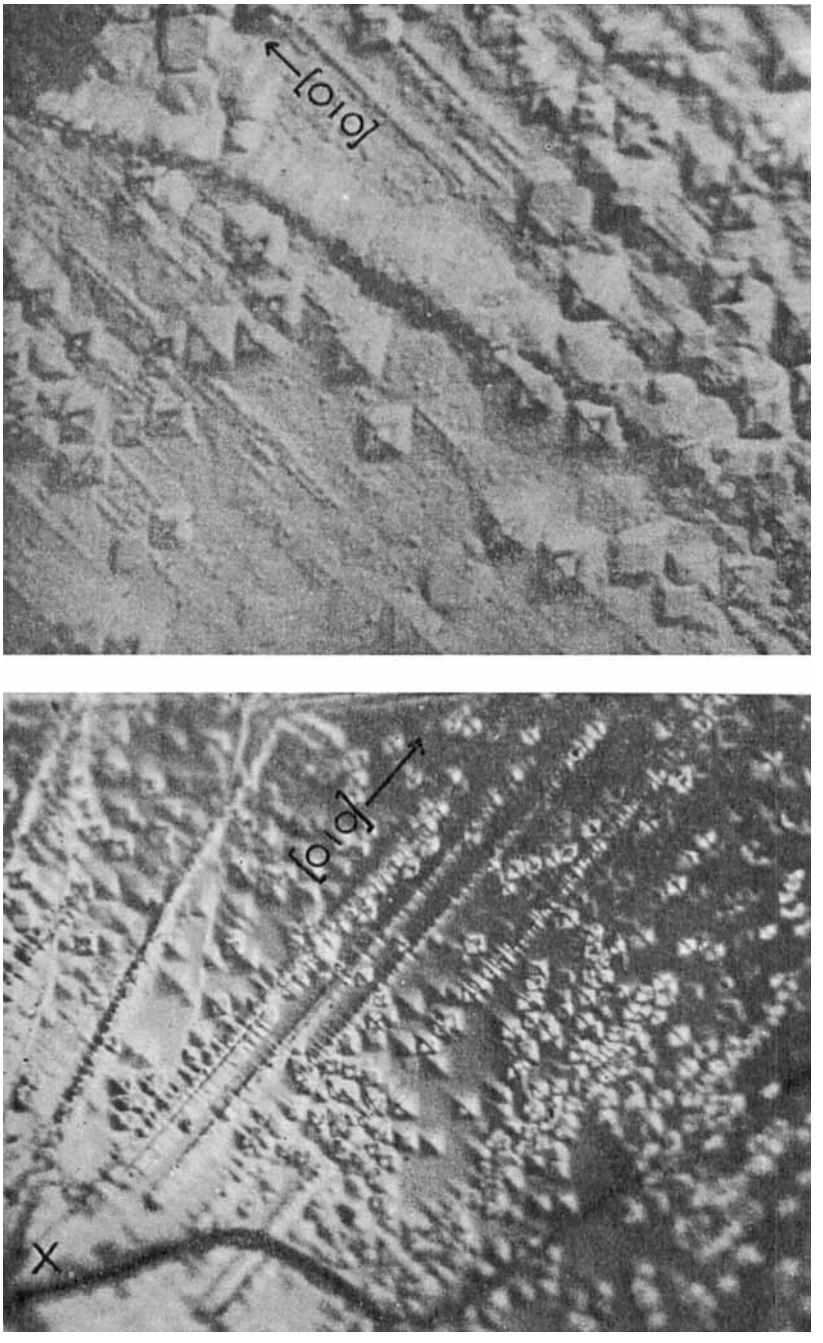

Figure 3. Micrograph of an etched (00*l*) face of anthracene after deformation by compression perpendicular to (010) planes. Note the two sizes of etch pits. (× 300)

Figure 4. Micrograph showing the region around a region Z where the (00*l*) face was indented. (× 300)

direction, have been shown‡ to be nucleated at the emergence points of dislocations introduced during the deformation. Bearing in mind the direction of compression and the observed alignments, it follows that these dislocations are of edge character and may be designated $\{h0l\}$ [010]. Figure 4 shows an etched cleavage face deformed by point indentation at the region marked X. Pronounced alignment of etch pits in the [010] direction may again be seen. But, on this occasion, there is no difference in size between pits nucleated at randomly distributed and "introduced" dislocations. Again, however, the aligned dislocations must be of the type $\{h0l\}$ [010].

The possibility exists that either different types of edge dislocations are introduced by the two methods of deformation, or the same type (same slip plane and *direction* of Burgers vector) is produced in each case but the *magnitude* of the Burgers vector is different. (The elastic strain energy of a dislocation is proportional to the square of the Burgers vector, and there is evidence[15] that pit size for given conditions of etching increases with increasing magnitude of the Burgers vector). The two most likely types of edge dislocation would, as mentioned in Section 2.2, be (100) [010] and $(20\bar{1})$ [010]. Both these would emerge at the $(00l)$ planes as pure edge dislocations, but the inclination of the dislocation line would be different (see Fig. 5).

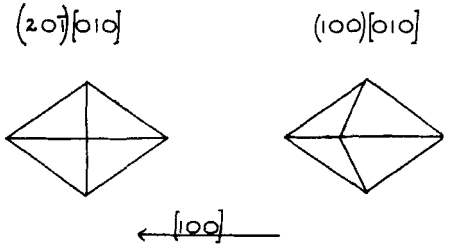

Figure 5. Schematic representation of shapes of etch pits expected at $(00l)$ faces from the two types of edge dislocations (100) [010] and $(20\bar{1})$ [010].

Whereas the edge dislocation that glides in a $(20\bar{1})$ plane in the [010] direction intersects the basal face at right angles, the edge dislocation gliding in a (100) plane intersects the basal face at an angle of *ca.* 55°, the supplement of the β-angle in anthracene. Consequently,[16]

‡ By first etching a sample, then deforming it and finally re-etching.

etch pits nucleated at $(20\bar{1})$ [010] would be totally symmetrical in their internal structure in contrast to those formed at (100) [010].

We have obtained evidence for these two types of etch pits: it can be seen from Fig. 4 that, by point indentation, the $(20\bar{1})$ family is introduced preferentially, as judged by the symmetry of the pits. Unfortunately, because of the tendency for larger pits to become flat-bottomed on prolonged etching,‡ accurate values of the degree

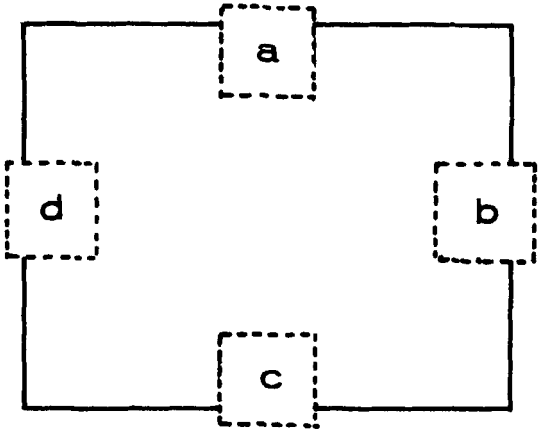

Figure 6. Schematic representation of regions photographed around the edges of a crystal deformed by cutting through the (00*l*) faces.

of asymmetry (for pits formed at dislocations introduced by compression) are not easily obtained; but angles of inclination of 50° to 60° for the dislocation line with respect to the basal plane have been obtained.

When a crystal is deformed by cutting through the (00*l*) faces with a blade, it is found that, if a rectangular section is removed (Fig. 6), at one pair of opposite edges (a and c of Fig. 6 and Figs. 7a and 7c) the $(20\bar{1})$ family of aligned edge dislocations tend to be introduced, whereas the (100) family is introduced at the other pair (b and d of Fig. 6 and Fig. 7b and d). The symmetrical pits have been marked *A* and *B* in Fig. 7a and c respectively. Note that the aligned pits in Fig. 7b and d are smaller, even though the same etching conditions prevail for all four regions.

Figure 8 shows another region of the crystal used in the previous

‡ It is likely that better etchants, such as that recently discovered by Robinson and Scott,[5] may yield more conclusive results.

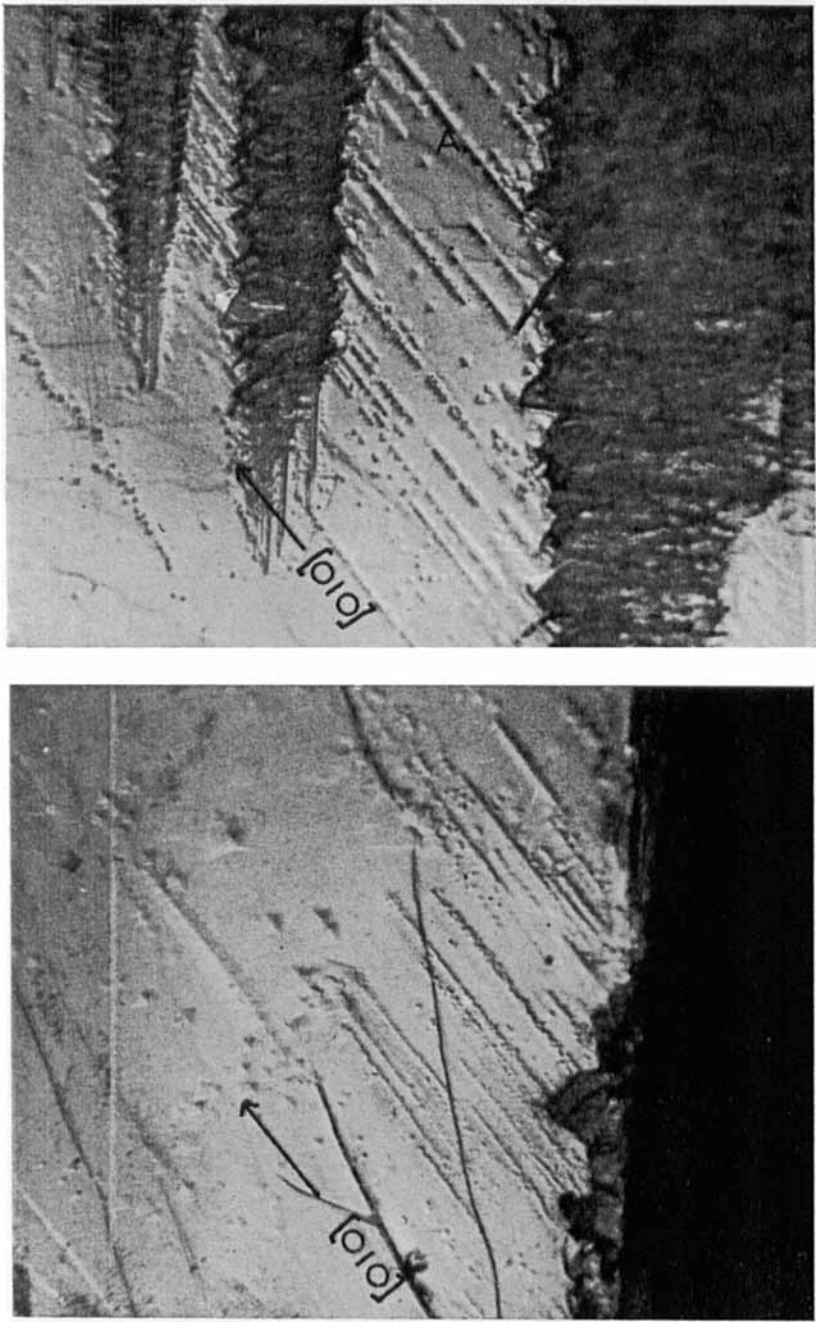

Figure 7a, b, c, d. Micrographs of regions shown in Fig. 6. Note the pronounced alignment of etch pits in [010] direction in each micrograph. (× 240)

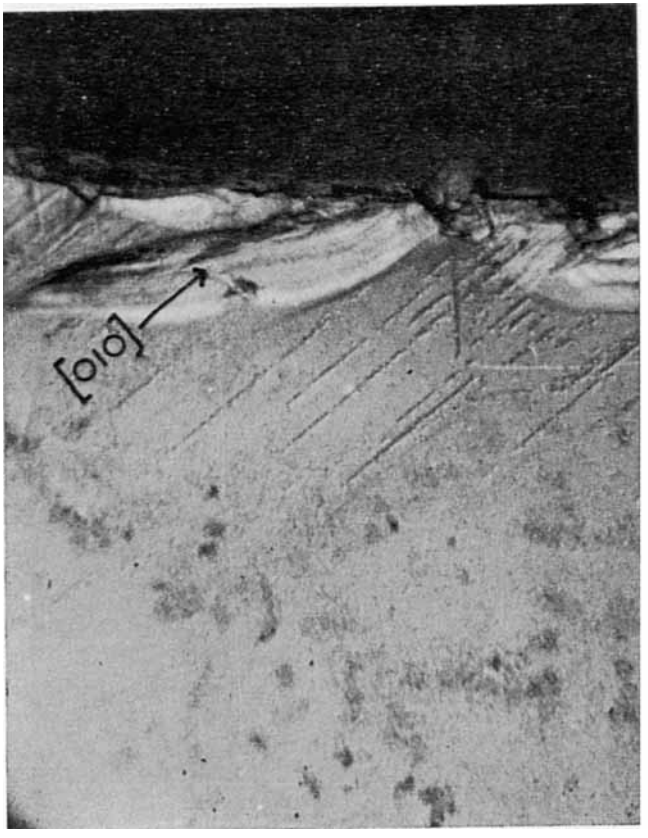

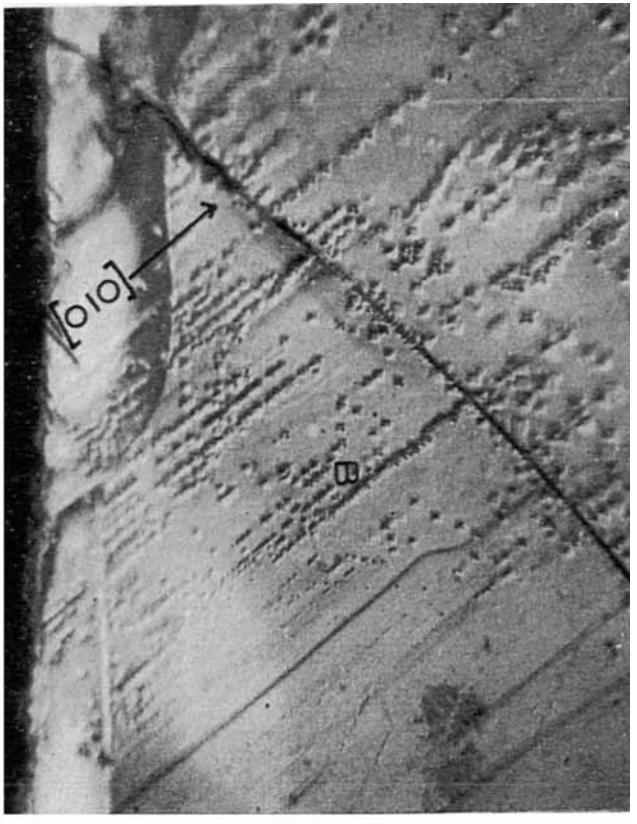

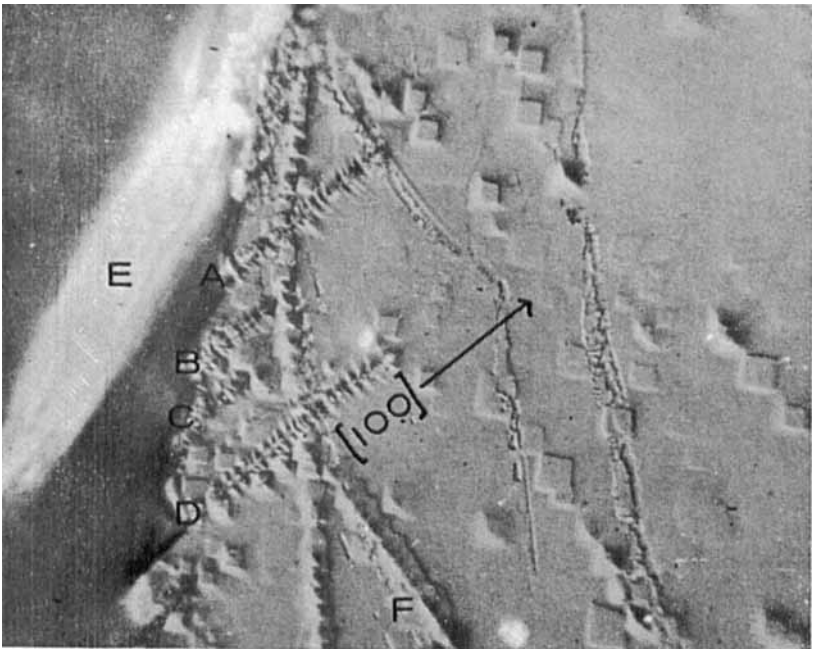

Figure 8. Alignment of etch pits in [100] direction probably representing glide polygonisation of edge dislocations. (× 600)

experiment. Etch pits aligned in the [100] direction (*A*, *B*, *C* and *D*) emerge from the region of a crack *E*, together with the (010) alignment *F*. We conclude that this [100] alignment represents glide (or mechanical) polygonization of the edge dislocations introduced during deformation. As pointed out by Livingston,[17] this type of polygonization is to be contrasted with that due to climb, which can only occur at relatively elevated temperatures. Glide polygonization has been observed in numerous ionic solids,[18,19] and also in another molecular crystal, sucrose.[20]

2.4. Comments on the Possibility of Other Non-basal Slip Systems

Another close-packed plane that intersects (00*l*) faces in anthracene is of the type $\{h10\}$ where h is 1 or $\bar{1}$. Slip might be possible in [001], or $[\bar{1}10]$ (or [110] when $h \equiv \bar{1}$) directions giving screw and edge dis-

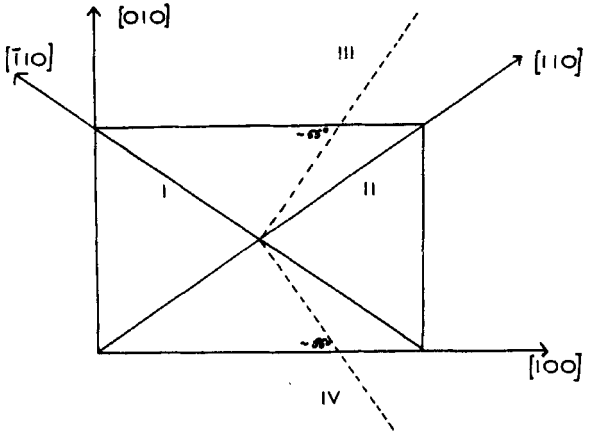

Figure 9. Diagram illustrating some of the directions of alignments expected if other non-basal slip systems were operative. (see text)

locations intersecting (00*l*) planes respectively. Both these would result in alignments of etch pits at (00*l*) faces in either [110] or [1̄10] directions. By the use of a diagram such as Fig. 9 it can be shown that symmetrical tilt boundaries resulting from polygonization of such edge dislocations should be aligned at 55° to the [100] direction (on (00*l*) faces), and that asymmetrical tilt boundaries arising from two sets of orthogonal edge dislocations are impossible for the two systems ((110) [1̄10] and (1̄10) [110]). Because we have never observed preferred alignment of etch pits along [110] and [1̄10] at (00*l*) faces—and several hundred crystals have been examined—we conclude that dislocations which glide on (110) or (1̄10) planes, are extremely rare. Furthermore tilt boundaries of the type shown in Figs. 10 and 11, which are inclined at 20° and 35° to the [100] direction respectively, may be satisfactorily explained on the basis of mutually perpendicular edge dislocations of type {*h*0*l*} [010] and (010) [100].

3. Electrical Measurements

It was felt that, because the dislocation content of melt-grown crystals of anthracene increases by about two orders of magnitude (to $10^7 - 10^8$ cm.$^{-2}$) on deformation by compression, electrical measurements on deformed samples might throw some light on the

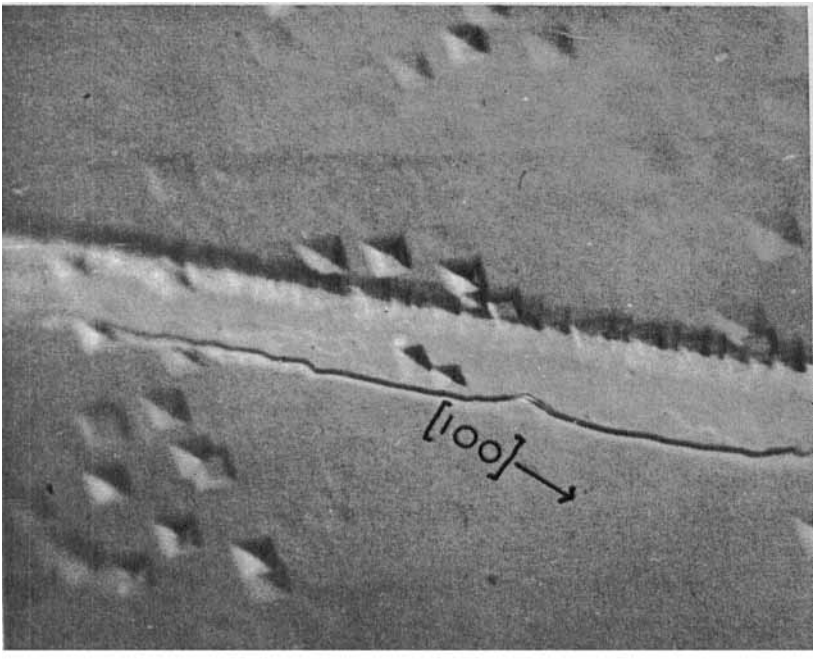

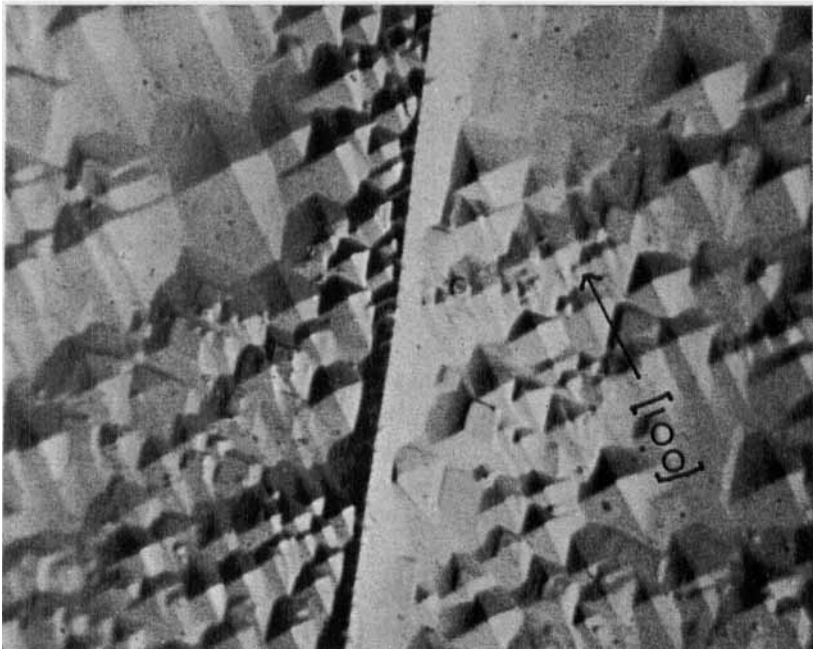

Figure 10. Asymmetric tilt boundary inclined at *ca.* 20° to [100] direction.

Figure 11. Asymmetric tilt boundary inclined at *ca.* 35° to [100] direction.

nature of carrier trapping in solid anthracene, a topic which has received much attention of late.[21-23] No effort was made to correlate the dislocation content with the straightforward d.c. conductivity, because the results of Riehl and others[24] had clearly demonstrated the profound influence of electrode material on this property. Two other approaches were adopted: the study of thermally-stimulated currents (conductivity-glow), and of space-charge-limited currents.

3.1. Thermally Stimulated Currents

We employed a modification of the technique and procedure used by Kokado and Schneider[25] in which a crystal is heated at a fixed rate in the dark after it has been illuminated by UV light at low temperature. The temperature corresponding to the occurrence of conductivity peaks depends on the energy of the carrier traps, and the intensity of the peak is proportional to the number of trapped carriers.

It was established, for vapour-grown, solution-grown, and melt-grown crystals, that genuine "glow-curve" phenomena were observed (see Thomas, Williams and Cox[26] for fuller details). In particular, from 180° to 373 °K there was but one peak centred at around 273 °K. This was taken[25-27] to be an indigenous feature of the behavior of anthracene, and not in any way related to the presence of tetracene or other impurity. Thus, in the region of the energy gap explored by this technique, there is but one trap energy. From the Gibson and Garlick[28] treatment of glow-current with temperature, the trap depth (assumed to be discrete, with no retrapping) was found to be 0.7 eV; and all our data were interpretable on the supposition, made also by Kokado and Schneider,[25] that it is positive holes which are being trapped (i.e., at a height of 0.7 eV above the valence band).

Rather unexpectedly, the magnitude of the peak height decreased by a factor of about six, when deformed crystals, containing 10^2 times as many non-basal dislocations as the ordinary melt-grown crystals, were used. If the peak at 273 °K is genuinely due to lattice defects of some kind,[25] this result is surprising. It must, however, be borne in mind that the "thermally-stimulated-current" technique, as employed by us, spans only a relatively small fraction of the entire band gap in anthracene. The actual trap energies detectable in our work lie between 0.4 and 1.1 eV. The observed decrease

in peak intensity could, therefore, be the consequence of the production of deeper traps by the introduction of the aligned non-basal dislocations. Alternatively, the extra dislocations may be effective recombination centers.

If it were possible to explore the whole of the energy gap, we could then discover whether the total number of carrier traps increases commensurately with the non-basal dislocation content. Space-charge-limited current measurements offer such a possibility, and the results of such studies are reported next. An additional advantage with space-charge-limited-currents is that traps throughout the bulk are investigated: with thermally-stimulated currents, because of the strong absorption of UV light during trap population, there is a tendency to overemphasize the role of surface traps.

3.2. Space-Charge-Limited-Currents

We adopted a procedure closely similar to that of Mark and Helfrich,[29] in which a modified[30] Kallmann and Pope[31] cell, consisting of aqueous iodide saturated with iodine as anode, was used. Such an anode is an effective injecting electrode, so that measurements of current-voltage dependences for four kinds of anthracene crystals (vapour-grown, solution-grown, melt-grown, and deformed melt-grown) could be readily made at room temperature. Mark and Helfrich[29] have shown that, when the total number of trapped carriers is appreciable and in excess of the total number of injected but free carriers, and provided there is an exponential distribution of traps (see Eq. (3) below), the steady-state current density j is given by:

$$j = N_0 \mu q^{(1-l)} \left\{ \frac{\epsilon \epsilon_0 l}{H(l+1)} \right\}^l \left(\frac{2l+1}{l+1} \right)^{l+1} \frac{V^{l+1}}{d^{2l+1}} \qquad (2)$$

Here, N_0 is the density of states of the energy band (2.5×10^{25} metres^{-3}); μ is the mobility of the charge carriers, q is the electronic charge, l is a dimensionless constant the value of which represents the state of disorder of the crystal under study (it is equal numerically to T/T_c—see Eq. (3)); ϵ and ϵ_0 are, respectively, the permittivity of anthracene and of free space; H is the total number of traps per unit volume; V is the voltage; and d the distance between the

electrodes (i.e., crystal thickness). Much independent evidence[23] exists which strongly suggests that the total number of trapping states per unit energy range and per unit volume $h(E)$ is approximately exponential, *i.e.*

$$h(E) = (H/kT_c)\exp(-E/kT_c) \tag{3}$$

where E is the depth of the trap (measured from the top of the valence band, since we are concerned with positive holes); k is Boltzmann's constant; and T_c has the dimension of temperature and characterizes the decrease of $h(E)$ with E.

Values of H and l were readily computed, using Eq. (2), from the slopes of log j versus log V plots. Table 1 summarizes the results obtained with the four kinds of crystal studied (the results of the " thermally-stimulated-current " studies are also included for comparison).

TABLE 1 Summary of Results Obtained from Measurements of Thermally-stimulated (TS) and Space-charge-limited (SCL) Currents

Nature of crystal	Density of non-basal dislocations (cm^{-2})	Peak height (TS) (10^{12} amp)	Average trap density H (SCL) (cm^{-3})	Disorder index l (SCL)
Vapour-grown	10^2	1.2	1×10^{13}	2.5
Solution-grown	10^3–10^4	3.0	3×10^{16}	1.9
Melt-grown	10^5–10^6	3.2	2×10^{18}	1.5
Deformed melt-grown	10^7–10^8	0.5	2×10^{19}	1.2

Judging by the success of the Mark and Helfrich[29] approach (Eq. (2)) in interpreting our results, we may conclude that there is essentially an exponential distribution of trapping levels for positive holes in anthracene, a result which, at first sight, contradicts the conclusion from " thermally-stimulated-currents " that there are discrete traps. More reliance must be placed on the conclusion drawn from space-charge-limited-current measurements, because, there, we explore the entire energy gap of 3.7 eV. The " discrete " traps must be seen as just a small part of the whole spectrum of traps actually present.

Table 1 clearly shows that there is a correlation between trap density (H) and the density of non-basal dislocations. Such a correlation has often been implied in previous discussions[27,32,33] of trapping of charge carriers and excitons in anthracene.

It is of interest to note that reasonable values of the trap densities may be evaluated on the assumption that all the molecules of anthracene situated within a certain radius r from the core of a non-basal dislocation acts as a trapping centre. Take the deformed melt-grown specimens which have about 10^8 dislocations intersecting 1 cm^{-2} of basal surface, and which, from measurements of space-charge-limited-currents, have a trap density of *ca.* 10^{19} cm^{-3}. Bearing in mind that a dislocation density of 10^8 cm^{-2} is equivalent to dislocation *lengths* of 10^8 cm per cm^{-3}, and that 2 molecules of anthracene are housed in a (unit cell) volume of 580×10^{-24} cm^{-3} we may write

$$\frac{2 \times 10^8 \pi r^2}{580 \times 10^{-24}} = 10^{19} \tag{4}$$

so that $r = 400$Å. Although rather large this is a realistic value, and is to be compared with the values of the radius of distortion ranging from 2 to 20 Å deduced[34] for potassium bromide, a much more compact structure.

4. Photodimerization at Lattice Defects

It has been known for a long time [35-39] that ultra-pure and de-oxygenated crystals of anthracene and some of its 9-substituted derivatives form stable dipara-anthracenes by photolysis with UV light. According to Schmidt and his co-workers,[40,41] the crystal structure of the monomer is a good guide to the geometrical structure of the dimer; and, applied to 9-cyanoanthracene, the structure more nearly pre-formed in the host lattice is the *cis* dimer, which is the substance expected principally on photolysis. Craig and Sarti-Fantoni[33] have shown, however, that, contrary to this topochemical preformation theory, it is the *trans* photodimers which are formed preferentially. The suggestion has, therefore, been made[33] that crystal defects may act as preferred centers for reaction, it being feasible that molecules of anthracene have their excitation energies reduced somewhat when they are displaced from regular sites in the lattice.

The crystal structure of unsubstituted diparaanthracene has recently been determined[42]: it is orthorhombic with $a = 8.13$, $b = 12.08$ and $c = 18.85$Å, there being four molecules to the unit cell. The formation of the photodimer is, therefore, accompanied both by a net decrease in crystal volume of about 20 per cent, and very considerable turmoil at the molecular level in the parent lattice. From previous, qualitative, descriptions[3] of the sites of emergence of dislocations, it would appear that, on purely geometrical grounds, dislocation cores—especially where they emerge at the basal surface—would facilitate the process of dimerization.

The nucleation of the photodimer within the monomer crystal may be conveniently followed using interference contrast microscopy (following Nomarski[43]) (see Fig. 12). It was, consequently, relatively convenient to test whether the sites of emergence of non-basal dislocations act as regions of enhanced reactivity. A series of separated halves (obtained by cleavage) of melt-grown crystals were treated in the following manner. One half was etched with oleum (see Section

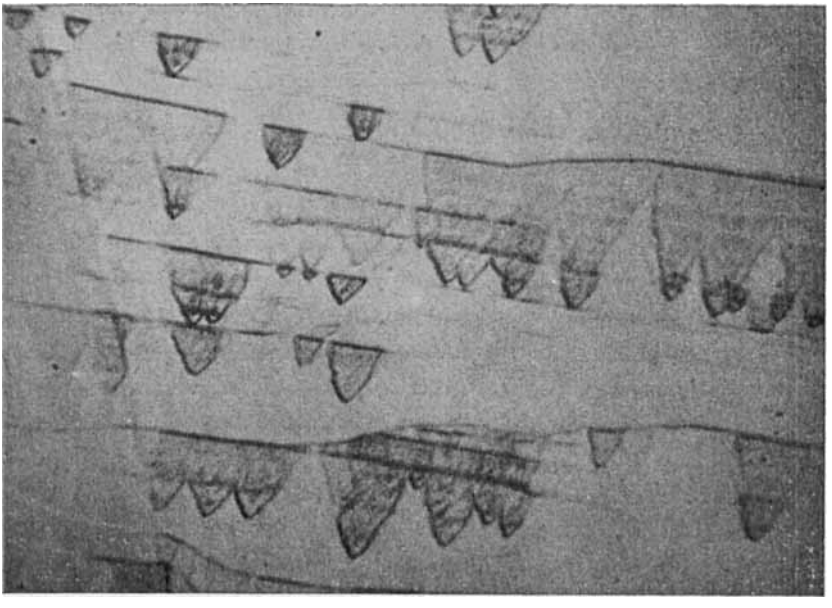

Figure 12. Interference contrast micrograph showing typical example of nucleation of photodimer within the anthracene crystal.

2 and ref. 3) to reveal the distribution of emergent dislocations; the other was photolyzed (in the absence of oxygen) with a medium-pressure mercury vapour lamp. Both aligned and isolated non-basal dislocations, as well as some surface steps, were found to favour photodimerization. Figures 13a and b and 14a and b show the degree of correspondence between etch pits on the one hand and dimerization centers on the other.

We may, therefore, draw the general conclusion that the topochemical preformation theory will not be of overriding importance in systems where there is enhanced reactivity at lattice imperfections.

We acknowledge the support of the Ministry of Technology and the kind interest and encouragement of Dr. L. J. Bellamy and Professor S. Peat.

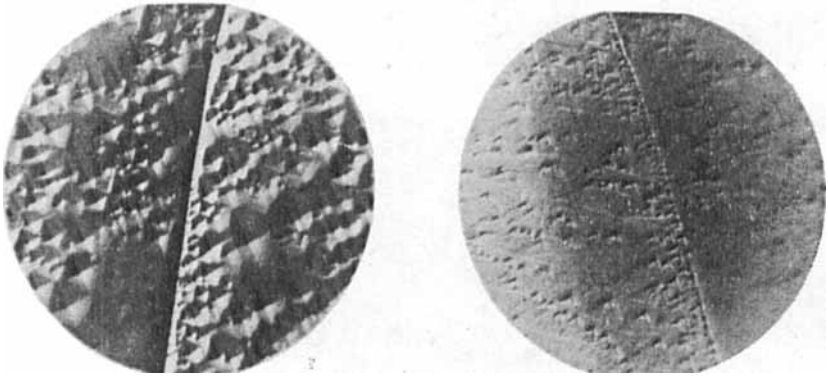

Figure 13. Pair of micrographs illustrating the degree of correspondence between etch pits on one cleavage face (a), and regions of preferred dimerization at the other (matched) cleavage face (b).

REFERENCES

1. McGhie, A. R., Reucroft, P. J. and Labes, M. M., *J. Chem. Phys.* **45** 3163 (1966).
2. Corke, N. T., Kawada, A. A. and Sherwood, J. N., *Nature* **212**, 62 (1967).
3. Williams, J. O. and Thomas, J. M., *Trans. Faraday Soc.* **63**, 1720 (1967).
4. Robinson, P. M. and Scott, H. G., *Phys. Status Solidii* **20**, 461 (1967).
5. Robinson, P. M. and Scott, H. G., *J. Crystal Growth* **1**, 67 (1967).
6. Sherwood, J. N. and White, D. J., *Phi. Mag.* **15**, 745 (1967).
7. Thomas, J. M. and Roscoe, C., *Chemistry and Physics of Carbon* (ed. P. L. Walker), (Marcel Dekker, New York, 1968) p. 1.
8. Gilman, J. J., Johnston, W. G. and Sears, G. W., *J. Appl. Phys.* **29**, 747, (1954).

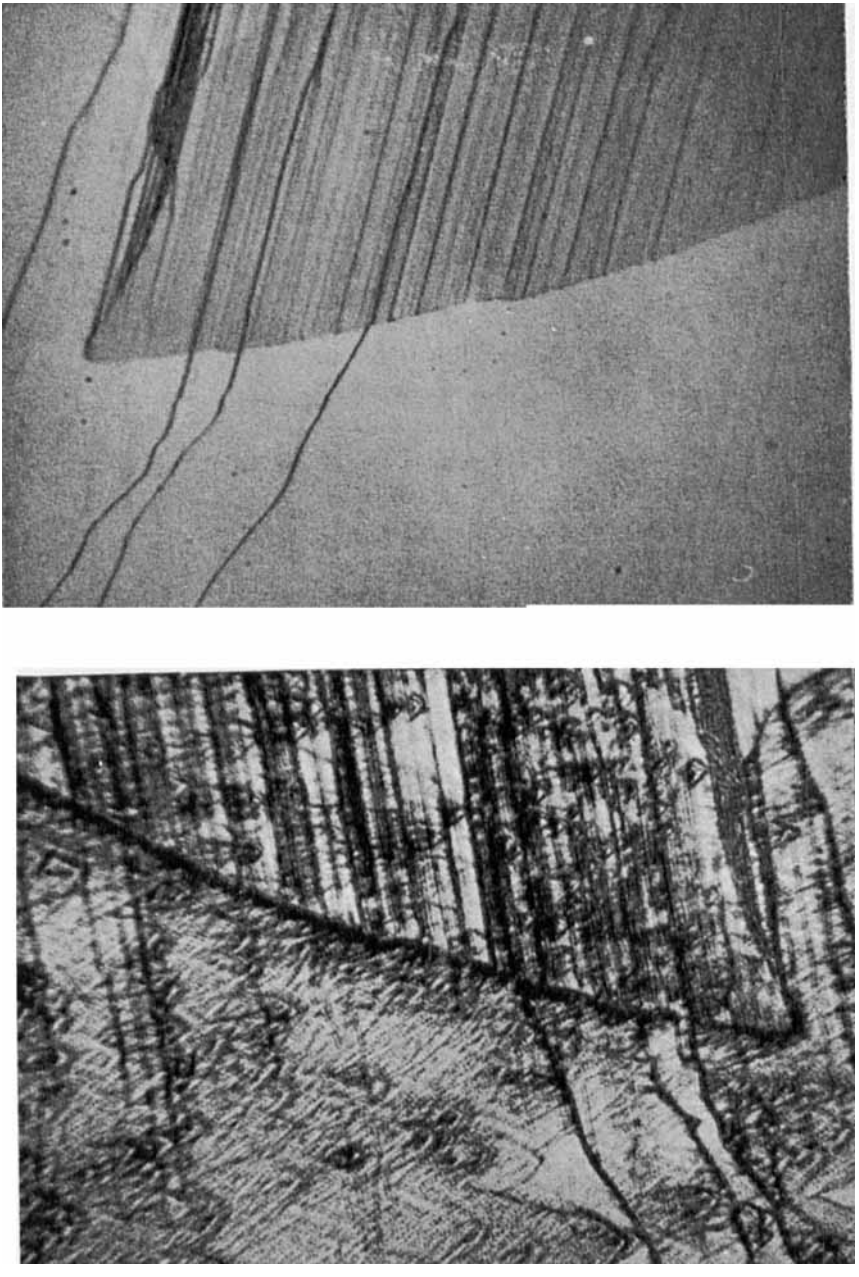

Figure 14. General correspondence between sites of emergence of non-basel screw dislocations (from which surface steps emanate) (a), and sites of preferred dimerization on the matched surface.

9. Davisson, J. W. and Levinson, S., *J. Appl. Phys.* **37**, 4888 (1966).
10. Gilman, J. J. and Johnson, W. G., *Dislocations and Mechanical Properties of Crystals*, (ed. J. W. Fisher, W. G. Johnston and R. Thomson) (J. Wiley, New York, 1957), p. 116.
11. Koffyberg, F. P., *J. Appl. Phys.* **36**, 844 (1965).
12. Thomas, J. M. and Williams, J. O., *Trans. Faraday Soc.* **63**, 1720 and 1922 (1967).
13. Thomas, J. M. and Renshaw, G. D., *J. Chem. Soc.* (A), 2058, (1967).
14. Frank, F. C., *Report of Pittsburgh Conference on Plastic Deformation of Crystals* (Washington–Carnegie Institute of Naval Research, 1950) p. 100.
15. Thomas, J. M. and Evans, E. L., *Nature* **214**, 167, (1967).
16. Johnston, W. G., *Progress in Ceramic Science* **2**, 1 (1962).
17. Livingston, J. D., *Acta Met.* **10**, 229 (1962).
18. Barber, D. J., Ph.D. Thesis, University of Bristol (1959).
19. Barber, D. J., *J. Appl. Phys.* **36**, 3342, (1965).
20. Thomas, J. M. and Williams, J. O., *Trans. Faraday Soc.* **63**, 1922 (1967).
21. Reucroft, P. J., Kronick, P. L., McGhie, A. R. and Labes, M. M., *Crystal Growth* (supplement to *J. of Phys. Chem. of Solids*) (Boston Conference, June, 1966) Paper B13. (Pergamon Press, Oxford, 1967).
22. Kronick, P. L. and Labes, M. M., *Mol. Crystals* **2**, 292 (1967).
23. Helfrich, W., and Lipsett, F. R., *J. Chem. Phys.* **43**, 4368 (1965).
24. Becker, G., Riehl, N. and Baessler, H., *Physics Letters* **20**, 221 (1966).
25. Kokado, H. and Schneider, W. G., *J. Chem. Phys.* **40**, 2937, (1964).
26. Thomas, J. M., Williams, J. O. and Cox, G. A., *Trans. Faraday Soc.*, in the press.
27. Bryant, F. J., Bree, A., Fielding, P. E. and Schneider, W. G., *Disc. Faraday Soc.* **28**, 48 (1959).
28. Garlick, G. F. J. and Gibson, A. F., *Proc. Phys. Soc.* **60**, 574 (1948).
29. Mark, P. and Helfrich, W., *J. Appl. Physics* **33**, 205 (1962).
30. Thomas, J. M., Williams, J. O. and Turton, L. M., submitted for publication.
31. Kallman, H. and Pope, M., *J. Chem. Phys.* **32**, 300 (1960).
32. Longuet-Higgins, H. C., *Disc. Faraday Soc.* **27**, 237 (1959).
33. Craig, D. P. and Sarti-Fantoni, *Chem. Comm.* 742 (1964).
34. Kawamura, H. and Okura, H., *J. Phys. Chem. Solids* **8**, 161 (1959).
35. Luther, R. and Weigert, F., *Z. Phys. Chem.* **51**, 297 (1905).
36. Wan, J. K. S., McCormick, R. N. and Pitts, J. N., *J. Amer. Chem. Soc.* **87**, 4409 (1965).
37. Chandross, E. A. and Ferguson, J., *J. Chem. Phys.* **45**, 3564 (1966).
38. Kei Sin Wei and Livingston, R., *Photochem. Photobiol.* **6**, 229 (1967).
39. Stevens, B., Sharpe, R. R. and Emmons, S. A., *Photochem. Photobiol.* **4**, 603 (1965).
40. Schmidt, G. M. J., in *Reactivity of Photoexcited Organic Molecules* (Proceedings of Solvay Conference) (J. Wiley, New York, 1967).
41. Cohen, M. D. and Schmidt, G. M. J., *J. Chem. Soc.* 1996 (1964).
42. Ehrenberg, M., *Acta Cryst.* **20**, 177 (1966).
43. Nomarski, G. and Weil, A. R., *Rev. Metal* (*Paris*) **52**, 121 (1955).